The Korean Journal of Rheology,
Vol. 6, No. 1, June 1994 pp. 30-40

〈연구논문〉

수렴관 유변측정기에서 K-BKZ 적분형 구성식을 사용한 M1 유체의 신장점도에 관한 연구

박헌진* · 김동회 · 이기준

*선경 인더스트리연구소
서울대학교 화학공학과

(1993년 11월 1일 접수)

A Study of Extensional Viscosity of Fluid M1 in Converging Channel Rheometer Using K-BKZ Integral Constitutive Equation

Hern-Jin Park*, Donhue Kim and Ki-Jun Lee

*R&D Center, Sunkyung Industries,
Department of Chemical Engineering, Seoul National University

(Received November 1, 1993)

요 약

고분자 물질의 신장점도(伸長粘度)를 측정하기 위하여 설계된 수렴관을 지나는 시험 유체 M1에 대하여 유한요소 방법으로 수치모사를 수행하였다. 구성방정식은 세 개의 이완시간을 가진 적분형 K-BKZ 모형을 사용하였다.

신장변형이 지배적이고 변형속도가 매우 큰 흐름에 대하여 실험적 방법으로 측정이 가능한 범위까지 수치모사를 수행하였다. 두 개의 압력 측정꼭지 사이의 벽면 압력차에 대하여 압력 신호로 측정한 실험값을 수치모사결과와 비교하였다. 겉보기 전단속도가 매우 큰 1300 s^{-1}에 이르는 높은 유속의 전 실험범위에 대하여 안정된 수치해를 얻을 수 있었다. 30℃에서는 모든 실험범위의 유속에서 압력차에 대한 수치모사 결과가 실험값과 잘 일치했다. 21℃에서는 0.1×10^{-3} m^3/s보다 낮은 유속범위에서 실험값과 일치하는 결과를 얻었으나, 그보다 높은 유속에서 실험값과 다른 경향의 결과를 얻었다. 이것은 낮은 온도 높은 유속 조건에서 M1 유체의 성질이 불안정하고, 또한 그러한 조건의 실험에서 발생한 압력 측정꼭지 부근의 기포들이 정확한 압력측정에 영향을 끼쳤기 때문이다. 수치모사 결과로부터 얻은 압력과 응력분포로부터 수렴관 유변측정기의 유동특성을 밝힐 수 있었다. 이는 실험적 방법을 통해서는 얻기 어려운 결과들로서 중요한 의미를 가진다. 특별한 모양을 갖도록 설계된 수렴관을 통과하는 M1 유체가 중심부근에서 일정한 신장변형속도로 변형됨을 확인할 수 있었으며, 수직응력은 지수적으로 증가하다가 축소부분을 지난 후 매우 서서히 감소하였다. 수치모사로부터 얻은 M1 유체의 신장점도를 실험결과와 비교하였다. 정상상태값에 접근한 신장점도를 얻기 위하여 신장변형속도가 일정한 구역이 두 배로 확장된 수렴관이 수치적으로 다루어졌고, 이를 통하여 기존의 수렴관에서 구한 값보다 큰 신장점도를 얻을 수 있었다.

Abstract—Numerical simulation has been undertaken for the flow of test fluid M1 passing through the converging channel system designed to measure the extensional viscosity of polymeric liquids. The constitutive equation is an integral-type K-BKZ model with three relaxation times. The simulations have been performed for the full range of experimental measurements in the system where the extensional deformation is dominant and the deformation-rates are very high. Stable solutions have been obtained for the whole experimental range even though the apparent shear rates reach 1300 s^{-1}. Results of the simulations concerning wall pressure difference between two pressure taps are compared with the experimental data measured from the pressure signals. The simulations are in good agreement with the experiments for the low range of flow rates at 21℃ and for all flow

rates at 30℃. The discrepancies at high flow rates of 21℃ is apparently due to the appearance of a stationary bubble in the experiments that may have altered the pressure measurements and the instability of fluid M1. The pressure and stress distributions from the simulations show the flow characteristics of the converging channel system, which are difficult to verify by using experimental methods. The specially designed converging channel geometry makes the fluid M1 deform at a constant rate of extensional deformation near the centerline within the constant strain rates section. The extensional viscosities of fluid M1 obtained by simulations have been compared with the ones from the experimental results. The results of extended channel, which has twice longer length of constant strain rate section than James' [1], are presented in order to obtain more developed extensional viscosity to steady state and to show the geometry effect on the flow characteristics.
Keywords: Extensional viscosity, convergingging channel rheometer, fluid M1, integral constitutive equation.

1. Introduction

One of the outstanding and well-recognized problems in the rheology of polymeric fluid systems is the measurement of extensional visco sity. Over the last two decades various techniques have been described to measure this property and specialist workshops have been conducted such as the recent one at Chamonix [2]. At this meeting it was soon apparent that the data from various instruments were significantly different partly because different fluids were utilized, and a pressing need for a cooperative measurement exercise on a single fluid was articulated. The comprehensive nature of the exercise immediately set constraints on the selection of the test fluid owing to widely different capabilities and limitations of different equipment. A test fluid which could satisfy these conflicting constraints was prepared at Manash University, which led to the fluid's being called M1. The fluid M1 consists of a 0.244% polyisobutylene in a mixed solvent consisting of 7% kerosene in polybutene. The preparation of the test fluid and the manufacturers' specification on the constituents are detailed by Nguyen and Sridhar [3].

In the present study, we examine an interesting system used in the M1 project, namely the flow through a converging channel so desinged as to allow measurement of the extensional viscosity of the polymer solution. The converging channel flow was developed by James et al. [1] to measure the step-input extensional viscosity denoted by η_E^+ [4]. In this case, the fluid undergoes no extensional deformation and then is suddenly subjected to a constant rate of extension. Their idea was to create this motion approximately by making the fluid pass through a converging channel particularly shaped. The first section of the channel is a cylindrical tube so that the extensional deformation can be taken as zero. The channel then converges smoothly over some distance so that the fluid within is extended at a constant rate. The converging channel is the only system so far which makes the fluid deform at a constant extensional deformation rate. In the other systems (fiber spinning, opposing jets, falling drop and open syphon and so on), the extensional rate is not constant at each position of deforming fluid in extensional viscosity measurement systems.

Park et al. [5] had tested this converging channel numerically and showed the flow characte ristics of it. Extensional viscosity directly calculated from their simulation results was presented and more reasonable method to calculate it from experimental data was proposed. The extensional viscosity obtained from converging channel is not a steady state value. Therefore the extended channel which has longer constant strain rate section is needed in order to obtain the values closer to steady state. The extended channel which has two times longer constant strain rate section than James' channel [1] is handled numerically.

Considerable success in modelling viscoelastic flows has been achieved recently with an integral constitutive equation of the K-BKZ type, proposed by Papanastasiou et al. [6]. This equation has been used to predict several well-known viscoelastic phenomena [7-10]. It has also been used for the modelling of the test fluid M1 by Chai and

Yeow [11], who give the parameter constants for this fluid at 21℃. They used this equation in the modelling of the gravity jet system for the fluid M1 with considerable success. Park and Mitsoulis [12] obtained reasonable results of circular entry flow of fluid M1 using the K-BKZ equation with the parameters determined by Chai and Yeow [11]. They showed that the geometry effects play an important role in the flow of viscoelastic fluids. Their solutions reached up to the limit of the experimental range with good convergence of the numerical scheme. The converging channel system was treated using the K-BKZ equation by Park et al. [5] and they obtained the quantitatively good results. The effect of extensional motion has been recognized as an important key factor to better understand and differentiate the flow behavior of polymer solutions and melts. Our study reveals the flow characteristics in the converging channel used to measure the extensional viscosity and the effect of the length of constant strain rate section on extensional viscosity.

2. Mathematical Modelling and Method of Solution

The converging channel flow is governed by the usual conservation of mass and momentum. For an incompressible fluid under isothermal conditions we have

$$\nabla\cdot\bar{v}=0, \tag{1}$$

$$\rho\bar{v}\cdot\nabla\bar{v}=-\nabla p+\nabla\cdot\bar{\bar{\tau}} \tag{2}$$

where $\bar{v}$ is the velocity vector, $\bar{\tau}$ is the extra-stress tensor, and p is the scalar pressure and ρ is the density. In the converging channel, Reynolds number is in about 10 order range and apparent shear rate is in 1000(s^{-1}) order range, therefore the inertia can not be negligible in equation (2) to obtain more reasonable solutions in spite of much time consuming and elaborating numerical scheme. The constitutive equation that relates $\bar{\bar{\tau}}$ to the deformation history is a K-BKZ equation proposed by Papanastasiou et al. [6] and further modified by Luo and Tanner [13] and is written as

$$\tau=\frac{1}{1-\theta}\int_{-\infty}^{t}\left[\sum\frac{a_k}{\lambda_k}\exp\left(-\frac{t-t'}{\lambda_k}\right)\right.$$

$$\left.\frac{\alpha}{(\alpha-3)+\beta I_C+(1-\beta)I_{C^{-1}}}\{C^{-1}(t')+\theta C(t')\}\right]dt' \tag{3}$$

where λ_k and a_k are the relaxation times and reaxation modulus coefficients at a reference temperature, α and β are material constants, and I_C, $I_{C^{-1}}$ are the first invariants of the Cauchy-Green tensor C and its inverse C^{-1}, the Finger strain tensor. θ is also material constant written as

$$N_2/N_1=\frac{\text{second normal stress difference}}{\text{first normal stress difference}}=\theta/(1-\theta) \tag{4}$$

and is not zero for the fluid which has a non-zero second normal stress difference. The fluid M1 passing through the converging channel is simulated with the θ value of $-1/9$.

The above constitutive equation is solved together with the conservation equations using the Finite Element Method (FEM) with a special numerical scheme to calculate the viscoelastic stresses for the general case of flows with and without recirculation [14]. Galerkin discretization is maintained and the numerical algorithm for convergence is Picard iteration as described in Ref. [14]. For constrained flows without free surfaces convergence has always been good even for very high flow rates. Convergent solutions have been obtained independent of mesh size, provided enough elements are used and the solution procedure advances slowly from low flow rates (Newtonian behavior) to higher ones by using a flow rate increment scheme [14].

3. Results and Discussions

Simulations for the test fluid M1 have been undertaken using the integral constitutive equation (3) with parameters determined by Chai and Yeow [6]. Table 1 shows the values of the parameters at various temperatures. With these parameters it is possible to fit well the linear vi-

Table 1. Material parameter values used in eqn. (3) for fitting data of fluid M1 at 21℃ according to Chai and Yeow [9] and values at 30℃ and 40℃ for fitting experimental data given by Binging et al. [16] and Hudson and Ferguson [17] ($\alpha=500$, $\beta=0.001$, $\theta=-1/9$, $\rho=900$ (at 21℃) and 826 (at 30℃) Kg/m^3)

k	λ_k (s) 21℃	a_k (Pa) 21℃	λ_k(s) 30℃	a_k (Pa) 30℃
1	1.04×10^{0}	5.50×10^{-1}	5.53×10^{-7}	5.50×10^{-1}
2	8.90×10^{-2}	5.46×10^{0}	4.73×10^{-2}	5.46×10^{0}
3	5.20×10^{-4}	3.06×10^{3}	2.77×10^{-4}	3.06×10^{3}

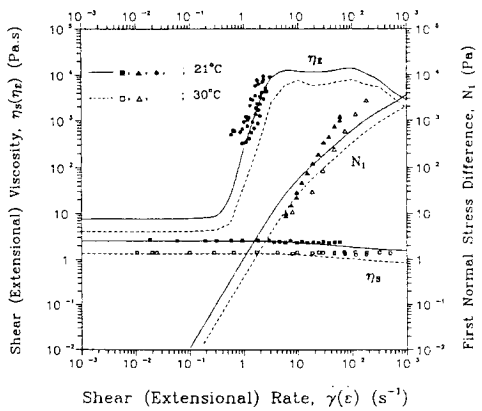

Fig. 1. Model prediction of shear viscosity, first normal stress difference, and extensional viscosity for fluid M1 using eqn. (3) with data given in Table 1. Closed symbols are experimental data given by Chai and Yeow [11] and open symbols are experimental data given by Binging et al. [16] and Hudson et al. [17].

scoelastic spectrum and also experimental data for the shear and extensional viscosities and the first normal stress difference [15-17] as shown in Fig. 1. Note that the same parameters at 21℃ have been used in previous studies [11,12], but in the present work an additional constant θ has been added to account for non-zero second normal stress difference coefficient exhibited by the M1 fluid according to experimental evidence [15,16].

Figure 2 represents the converging channel geometry as given by James et al. [1]. All dimensions are given in millimeters. There are two cylindrical sections in the inlet and outlet of the domain. The conical section follows the inlet cylindrical section and induces the fluid to pass though the constant strain rate section. There the channel converges smoothly over some distance so that the fluid within is extended at a constant rate. In using converging channel flow for extensional rheometry, the flow rate has to be high in order to confine the shear effects to the wall region and to create a core flow which is nearly free of shearing and in which extensional deformation is more dominant than shear deformation.

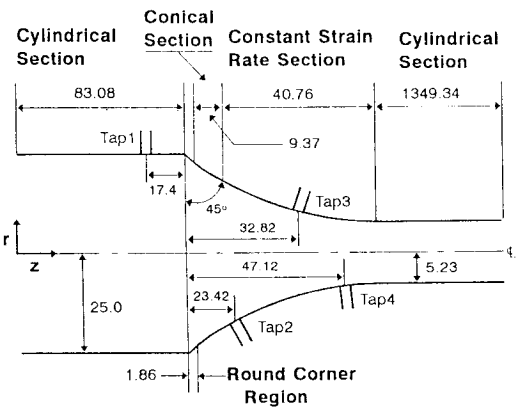

Fig. 2. System configuration of the converging channel used in the measurement of extensional viscosity of M1 by James et al. [3]. All dimensions are in millimeters and the shape of the constant strain rate section is given by $r^2(z-90.10)=1302$ mm^3.

Partial view of the finite element mesh used in the simulation is shown in Fig. 3. Mesh in Fig. 3(a) has the same geometry with James' channel [1], but the second channel in Fig. 3(b) is extended in order to obtain more developed extensional viscosity. The real mesh of Fig. 3(a) has the value of z from $-15.885R_o$ to $268R_o$. Such lengths were required in order to obtain fully developed entry and exit profiles and total relaxation of stresses in the downstream direction. Convergence was good for the whole experimental range of measurements.

The values of pressure drop are presented in terms of the pressure coefficient Cp and Re. Cp is $\Delta p/\frac{1}{2}\rho V^2$, where ΔP is the pressure drop between the two taps (from tap 1 to tap 3, or from

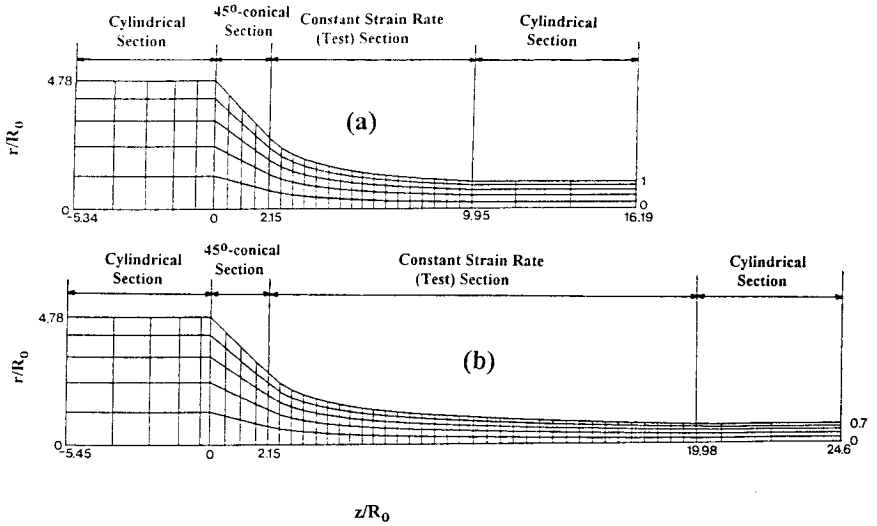

Fig. 3. Partial view of the finite-elements used in the simulations of the converging channel system: (a) James' channel, and (b) extended channel.

tap 1 to tap 4) and V is the mean velocity at later tap. The numerical results are presented in Fig. 4 and 5, together with the prediction from the generalized Newtonian solution by James et al. [1]. Our results of Newtonian fluid are nearly the same with the generalized Newtonian solution. For the non-Newtonian viscoelastic M1 fluids, the pressure coefficient Cp vs. Re is compared with James' experimental data. The results of simulation are in good agreement with James' experiments within small error limits. Although the peculiar phenomena of M1 fluid at 21℃ [1], the data show the same tendency that Cp decreases with increasing Re.

In this study, the results from simulation are compared using dimensional values with the experimental data obtained by James et al. [18]. Instead of giving dimensionless values (such as pressure coefficients Cp and Reynolds number Re), the dimensional values for the wall pressure drop between taps and for the flow rate are presented in order to offer a better quantitative comparison with the experiments. The simulation fits reasonably well with the experimental data as shown in Fig. 6, where (a) and (b) correspond to wall pressure drops between taps 1 and 3 and between taps 1 and 4, respectively. At higher flow rates, the experimental results show a peculiar behavior in which pressure drop decreases with increasing flow rate. This behavior at 21℃ is contrary to the general flow phenomenon. It may be due to probable instabilities occuring with fluid M1 at high flow rates and low temperatures. McKinley et al. [19] have shown in the contraction flow that such polymer solutions become unstable at some intermediate flow rate ranges and may revert back to stable at higher flow rates. A numerical solution based on the assumption of steady state cannot take into account such phenomenon.

This is apparently not the case at 30℃, where both simulations and experiments show a monotonic increases of the pressure drop with flow rate, as evidenced in Fig. 7. When the flow rates are less than $1.0\times10^{-3}m^3/s$ for 30℃, the results are virtually identical with the experimental measurements. The discrepancies between simulations and experiments are small for flow rates higher than $1.0\times10^{-3}m^3/s$. Thus the simulation provides quantitatively agreeable results of M1 fluid behavior in the converging channel system.

Simulations also provide some useful extra information, which is rather difficult to obtain experimentally. James et al. [18] designed the con-

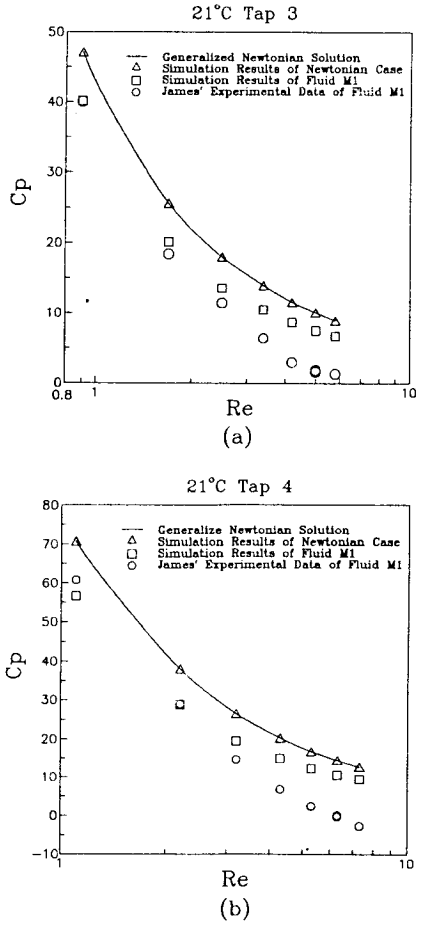

Fig. 4. Pressure coefficient (Cp) as a function of Reynolds number (Re) in comparison with generalized Newtonian solution and James' experiments [18] at 21℃: (a) Cp from tap 1 and 3, and (b) from tap 1 and 4.

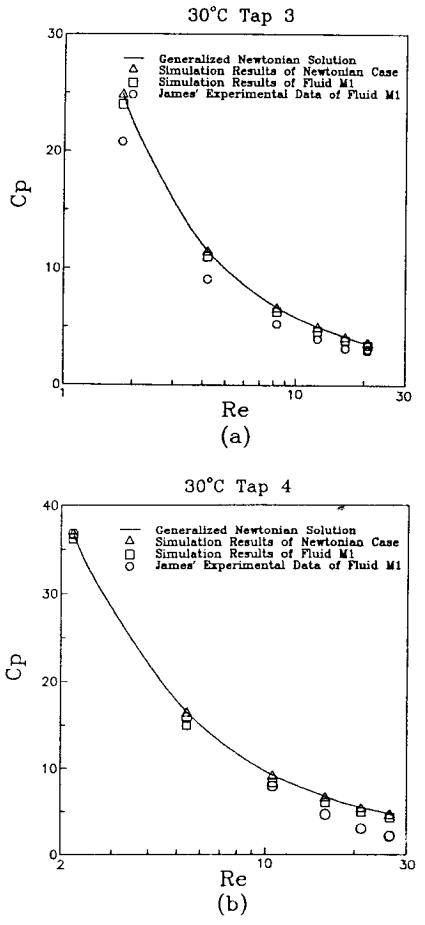

Fig. 5. Pressure coefficient (Cp) as a function of Reynolds number (Re) in comparison with generalized Newtonian solution and James' experiments [18] at 30℃: (a) Cp from tap 1 and 3, and (b) from tap 1 and 4.

verging channel such as to have the fluid deformed at a constant rate of extension. In the constant strain rate section, the velocity at the centerline when plotted as a function of axial distance, gives nearly constant slopes within the test section, as depicted in Fig. 8. Thus the fluid M1 is deformed at a constant rate of extension near the center region within the test section. The slope represents the extensional deformation rate and its value is large when the flow rate is high as was the case in the experiments in Fig. 9. When the flow rate is high, the inlet and outlet region in the constant strain rate section have the disaccording values of strain rate ($\dot{\varepsilon}$) in Fig. 9. In the case of relatively low flow rate, the strain rate ($\dot{\varepsilon}$) is constant in whole range of constant strain rate section. In the case of extended channel, the axial distance which shows constant strain rate is prolonged about two times longer in comparison with the James' channel.

The first normal stress difference of short and extended channel at the centerline is nearly zero before the 45°-conical section, as shown in Fig. 10. However, it increases exponentially in the conical section and the converging test section, then is slowly relaxed in the outlet cylindrical

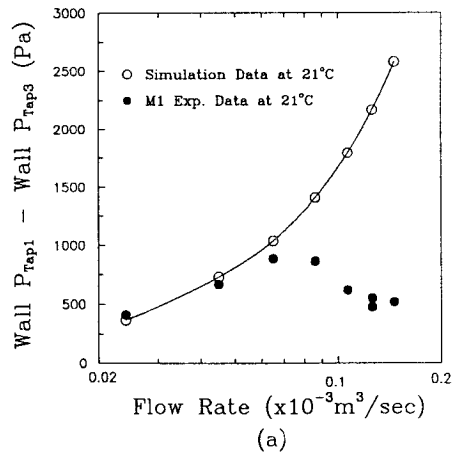

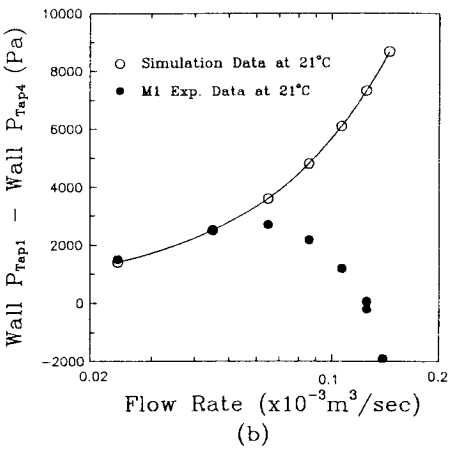

Fig. 6. Pressure drop between two taps as a function of flow rate in comparison with the experimental results by James et al. [18] at 21℃: (a) pressure drop between tap 1 and 3, and (b) between tap 1 and 4.

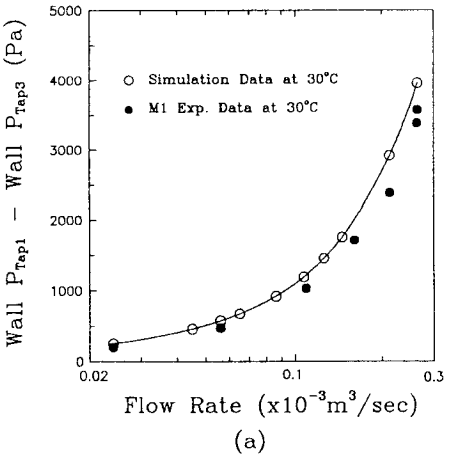

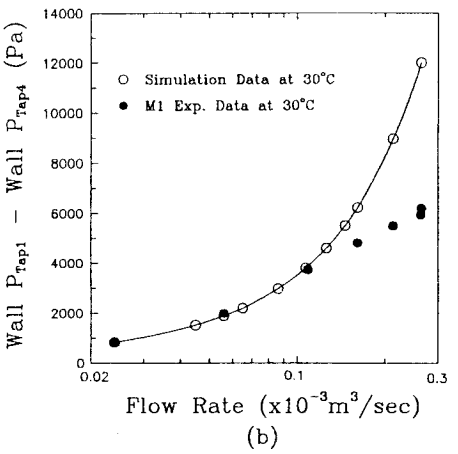

Fig. 7. Pressure drop between two taps as a function of flow rate in comparison with the experimental results by James et al. [18] at 30℃: (a) pressure drop between tap 1 and 3, and (b) between tap 1 and 4.

section to recover from its previously extensionally deformed state. And the values of extended channel increase continuously in the longer range of axial distance.

Shear stress contours are presented in Fig. 11 and show that the region where the maximum occurs is at the wall at the end of the constant strain rate section, because the shape of the channel after this section does not subject the fluid to any extensional deformation. The values of extended channel in Fig. 11(b) are greater than that of James' channel. The narrower geometry of extended channel in the down stream is the cause of high shear stress values. First normal stress difference contours are presented in Fig. 12. The minimum region is confined to the wall at the end of the 45°-conical section because the contracting shape of the channel makes the fluid elements to be contracted in the flow direction. The values increase rapidly in the constant strain rate section and have a maximum near the end of this section because the fluid elements within this section are extended in the flow direction. The contours of N_1 of short and extended channel show almost the same values near the 45° conical section, but value of N_1 is very high in the

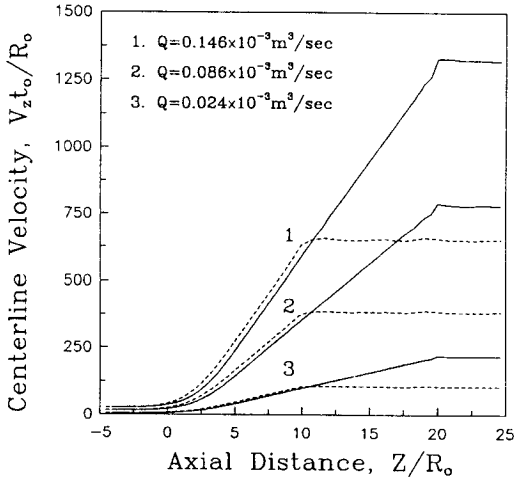

Fig. 8. Centerline velocity of fluid M1 as a function of axial distance for different flow rates at 21℃. The dashed and solid lines represent James' and extended channel, respectively.

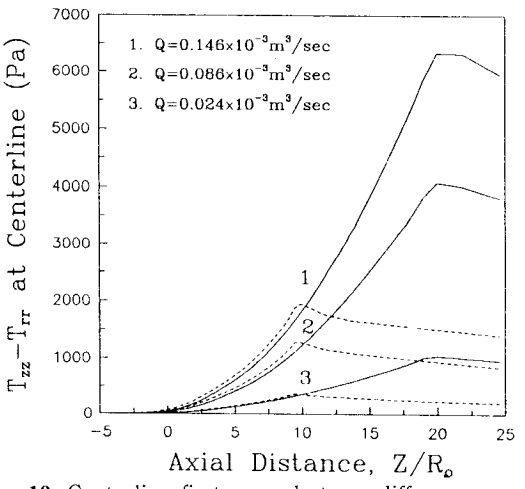

Fig. 10. Centerline first normal stress difference as a function of axial distance for different flow rates at 21℃. The dashed and solid lines represent James' and extended channel, repectively.

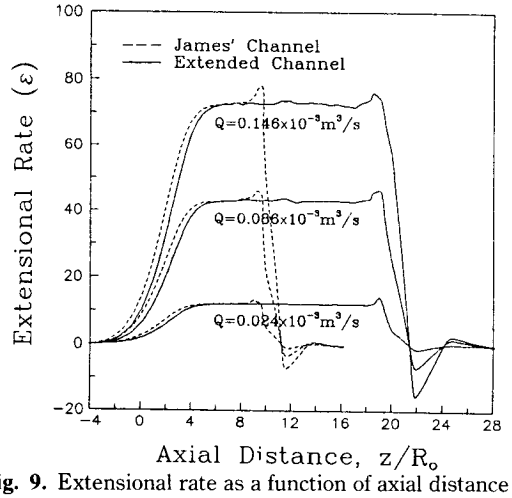

Fig. 9. Extensional rate as a function of axial distance for different flow rates at 21℃. The dashed and solid lines represent James' and extended channel, respectively.

stress difference exhibits larger value than the downstream of extended channel in Fig. 12(b). In the constant strain rate section, the first normal shear stresses.

The extensional viscosities plotted in Fig. 13 are step-input extensional viscosities η_E^+ [1, 4]. But in this paper η_E is used for η_E^+ without any distinction. The values of η_E are directly calculated from the simulation results of stress values τ_{zz} and τ_{rr}, and $\dot{\varepsilon}(=\partial v/\partial z)$ at centerline. The viscosity in Fig. 13 is not steady state value. Therefore it is developing toward steady state with increasing axial distance. In the James' channel, the values of η_E develop up to the axial distance 9 at which the constant strain rate section is ended in Fig. 13(a). But the extended channel gives us higher extensional viscosities, as depicted in Fig. 13(b).

The extensional viscosities from extended channel are presented as a function of extensional rate ($\dot{\varepsilon}$) in Fig. 14. It increases with axial distance, and shows slightly extension thinning in the case of small value of axial distance. According to the increasing axial distance, the extension thickening effect appears in 10~50 of $\dot{\varepsilon}$. The extension thinning might be due to unsteady state values of extensional viscosity. Up to now, we can be sure whether the steady state extensional viscosity is decreasing or increasing with strain rate. Another cause of extension thinning is the fact that no one knows the extensional viscosity of true steady state, thus the apparent extensional viscosities from fiber spinning data are used as steady state values under pure uniaxial extensional flow condition to determine the material parameters in K-BKZ equation (3). The steady state value of

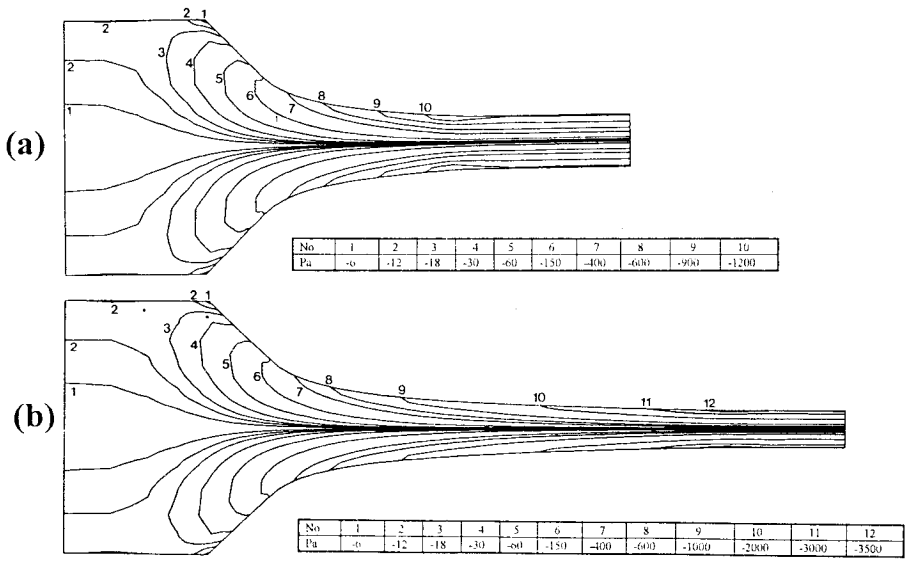

Fig. 11. Shear stress contours in the converging channel for flow rate of 0.086×10^{-3} m^3/s at 21℃: (a) James' and (b) extended channel.

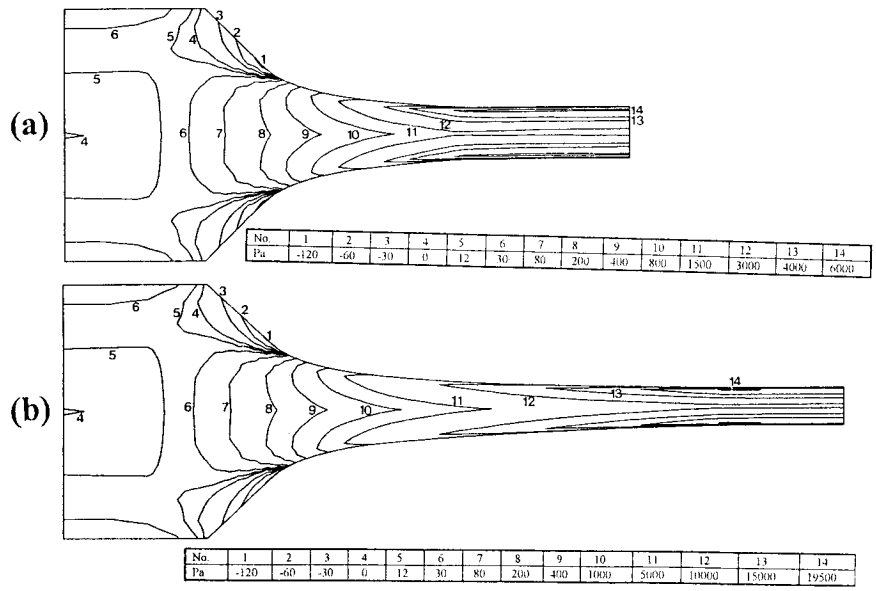

Fig. 12. First normal stress difference contours in the converging channel for flow rate of 0.086×10^{-3} m^3/s at 21℃: (a) James' and (b) extended channel.

K-BKZ model under simple uniaxial flow condition are nearly constant in the range of extensional rate 10~100 in Fig. 1. This effect also might influence the extension thinning behavior. Nevertheless, a more study is needed to find the more developed extenstional viscosity of steady state.

4. Conclusions

Numerical simulation for the flow of the test fluid M1 has been successfully carried out in the converging channel where the extensional deformation is dominant and the deformation rates are very high. The working constitutive equation was

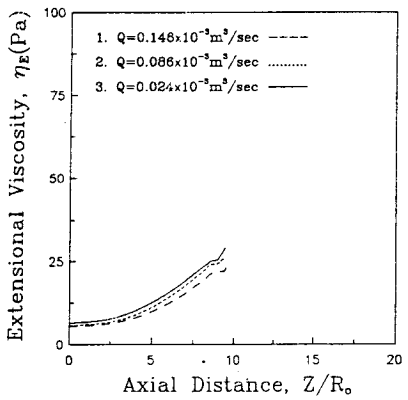

Fig. 13. Extensional viscosity as a function of axial distance at 21℃: (a) James' and (b) extended channel.

an integral-type K-BKZ model with a spectrum of three relaxation times.

Stable solutions have been obtained in the high flow behavior of fluid M1 which is due to the unstable flow rate ranges where the experimental measurements were available. The results of the simulation agree well with the experimental data by James et al. [1] for all flow rates at 30℃ and at low flow rates at 21℃. However, at high flow rates at 21℃ the simulations could not show peculiar.

The test fluid M1 shows a constant extensional deformation rate at least near the centerline in the constant rate section of the converging channel. The extended channel provides the longer region in which the extensional strain rate is contant. The first normal stress difference increases exponentially in both the 45°-conical section and the constant strain rate section, and is relaxed slowly in the last cylindrical section. In the test section where the pressure taps were located, the normal stresses are larger than the shear stresses, consequently the extensional deformation is dominant.

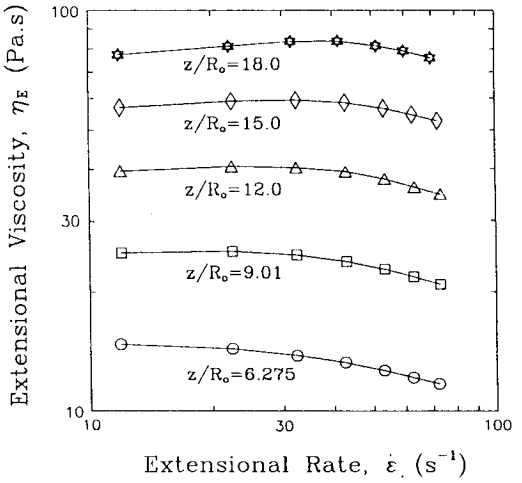

Fig. 14. Extensional viscosity as a function of extensional rate for different axial distance of extensional channel at 21℃.

Extensional viscosity directly calculated from the simulation results is obtained, and it increases with the axial distance. The extended channel provides more developed extensional viscosity.

Acknowledgements

Financial assistance from the Honam Oil Refinery Co., Ltd. is gratefully acknowledged.

References

1. D.F. James, G.M. Chandler and S.J. Armour, *J. Non-Newtonian Fluid Mech.*, **35**, 421 (1990).
2. Special Issue on Chamonix Conference, *J. Non-Newtonian Fluid Mech.*, **3**, 1 (1988).
3. J.M. Marchal and M.J. Crochet, *J. Non-Newtonian Fluid Mech.*, **26**, 77 (1987).
4. J.M. Dealy, *J. Rheol.*, **28**, 181 (1984).

5. H.-J. Park, D Kim, K.-J. Lee and E. Mitsoulis, *J. Non-Newtonian Fluid Mech.*, submitted (1993).
6. A.C. Papanastasiou, L.E. Scriven and C.W. Macosko, *J. Reol.*, **27**, 387 (1983).
7. X.-L. Luo and R.I. Tanner, *J. Non-Newtonian Fluid Mech.*, **22**, 61 (1986).
8. S. Dupont and M.J. Crochet, *J. Non-Newtonian Fluid Mech.*, **29**, 81 (1988).
9. X.-L Luo and E. Mitsoulis, J. Rheol., 33, 1307 (1989).
10. X.-L. Luo and E. Mitsoulis, *J. Rheol.*, **34**, 309 (1990).
11. M.S. Chai and Y.L. Yeow, *J. Non-Newtonian Fluid Mech.*, **35**, 459 (1990).
12. H.J. Park and E. Mitsoulis, *J. Non-Newtonian Fluid Mech.*, **42**, 1 (1992).
13. X.-L. Luo and R.I. Tanner, *Int. J. Num. Meth. Eng.*, **25**, 9 (1988).
14. X.-L. Luo and E. Mitsoulis, *Int. J. Num. Meth. Fluids*, **11**, 1015 (1990).
15. M.L. Chirinos, P. Craln, A. S. Lodge, J. L. Schrag and J. Yaritz, *J. Non-Newtonian Fluid Mech.*, **35**, 105 (1990).
16. D.M. Binging, D.M. James and K. Walters, *J. Non-Newtonian Fluid Mech.*, **35**, 121 (1990).
17. N.E. Hudson and J. Ferguson, *J. Non-Newtonian Fluid Mech.*, **35**, 159 (1990).
18. D.F. James, G.M. Chandler and S.J. Armour, *J. Non-Newtonian Fluid Mech.*, **35**, 445 (1990).
19. G.H. McKinley, W.P. Raiford, R.A. Brown and R.C. Armstrong, *J. Fluid Mech.*, **223**, 411 (1991).